INTERNATIONAL JOURNAL OF ENERGY STUDIES

Aerodynamic analysis of car rear spoiler with computational fluid dynamics for different angles and profiles

Muhammed Ali Oztemel[a], Fatih Aktas[b*], Nuri Yucel[c]

[a]*Department of Mechanical Engineering, Faculty of Engineering, Gazi University, Ankara 06570, Türkiye, ORCID:0009-0006-4868-3818*

[b] *Department of Mechanical Engineering, Faculty of Engineering, Gazi University, Ankara 06570, Türkiye, ORCID:0000-0002-1594-5002*

[c] *Department of Mechanical Engineering, Faculty of Engineering, Gazi University, Ankara 06570, Türkiye, ORCID: 0000-0001-9390-5877*

(*Corresponding Author: fatihaktas@gazi.edu.tr)

Highlights

- C_D and C_L values were investigated by numerical methods.
- Aerodynamic analysis of two different spoiler geometry.
- Comparison of C_D and C_L values for different airfoils, angel of attacks, and velocities.

ABSTRACT

The aim of the study is to compare the drag coefficient, downforce coefficient, and downforce created by the spoiler by analyzing them with the help of the Computational Fluid Dynamics (CFD) program at different wing profiles, different angles of attacks, and speeds. Solidworks was used to create the geometry for CFD analysis. ANSYS Fluent was used as the CFD analysis program. Two airfoil profiles BE153-055 and BE153-175, were selected for analysis to compare different airfoil profiles. Selected airfoils were placed at 10° and 20° angles of attack to compare different angel of attacks and analyzed at 30 (m/s), 50 (m/s) and 70 (m/s) velocities to compare different velocities. According to the analysis results, it was observed that downforce increased in direct proportion to the camber line, angle of attack, and speed. The highest downforce was obtained in BE153-175 airfoil, 20 degrees angle of attack, and 70 (m/s) speed.

Keywords: Airfoil, Downforce, Computational fluid dynamics (CFD), External flow

1. INTRODUCTION

Automobile aerodynamics are critically important in today's society. By enabling the analysis of the fluid flow surrounding a moving piece, aerodynamic work can help with maximum output [1]. A spoiler is an accessory component frequently found on fast automobiles that disperses the negative fluid motion around a body. These are employed to lessen turbulence caused by a pressure differential at the vehicle's back [2]. The speed limitations of modern motor vehicles are rising along with technological advancements and improvements to internal combustion engines' combustion systems. With increasing speeds, the control of motor vehicles becomes more complex and can cause unexpected accidents. This essentially illustrates the need to invent an aerodynamic wing that creates a carefully controlled stall on the wing part downwind and reduces the lift of that wing part. The spoiler is designed to reduce lift and significantly increase drag [3].

Drag force can be defined as the resistance of an object in a fluid medium to move in this medium. The drag coefficient of a solid body moving in any liquid or gas medium is directly proportional to the drag force. Therefore, the drag coefficient should be taken into account and considered as a critical feature when designing solid bodies moving in fluid media. The drag force is always opposite to the object's travel direction. The vehicle must have a drive system to overcome the drag force and accelerate sufficiently for the vehicle to move in a fluid medium. Keeping the drag force low is crucial regarding fuel cost and efficiency [4].

On the two sides of the wing, the airflow traveling at different speeds is differentiated under pressure, resulting in the physics rule known as Bernoulli's Principle. As this pressure tries to stabilize, the wing tries to move forward under lower pressure. While airplanes use wings to lift themselves up, racing cars use them for downforce, to keep them in place [4]. Downforce can be defined as the force required for the vehicle moving in a fluid environment to hold on to the ground and move without slipping, in other words, negative lift, pushes the car onto the track. Downforce becomes more critical at high speeds because the vehicle's downforce decreases at high speeds due to the geometric structure of the vehicle. Especially when it comes to corners, about 4 times the g acceleration is felt on an average Formula 1 car. For the car to turn the corner smoothly, it needs to produce a downforce force that will allow it to hold on to the ground despite the force of about 4g [4].

Based on an analysis of a vehicle with and without a spoiler, it was found that spoilers have a significant effect on the performance of a hatchback. As a result of the analysis, the drag coefficient increased by 8.33% with the addition of the spoiler and the lift coefficient decreased by 59.09% with the addition of the spoiler [5]. Improving the aerodynamic performance of the wing section is achieved by increasing the lift force generated around the wing section and reducing the drag force. The lift force is increased by giving the wing section a hump, which increases the drag force. This situation is observed when there is a non-symmetrical wing with a larger camber than symmetrical ones [6]. The primary configurations examined encompass a baseline flat-underfloor design, a 7° venturi diffuser-equipped setup, a venturi diffuser with diagonal skirts, and the same venturi diffuser with frontal slot-diffusers. Numerical predictions, evaluated through RANS Computational Fluid Dynamics (CFD) simulations, are focused on aerodynamic coefficients. The configuration that achieved the highest downforce coefficient was the model composed of a 7° venturi diffuser equipped with diagonal sealing skirts, attaining a C_L value of -0.887, representing an approximate 1780% increase compared to the baseline model [7]. Another study in the literature focuses on examining the fluid flow interaction around a bluff body to generate aerodynamic forces, including drag and lift forces. This research aims to simulate the fluid flow past a bus body with different diffuser angles on the rear. The diffuser angles were set at 0°, 6°, 12°, and 18°, respectively. CFD simulation results demonstrate that the installation of diffusers at the rear of bus body models can enhance aerodynamic forces, and the wake structure is in line with the increase in diffuser angle. The drag coefficient was reduced by up to 2.3% when associated with a 180° diffuser angle. Additionally, a 120° diffuser angle significantly increased downforce, showing a tenfold increase compared to the zero diffuser angle [8]. A different study focused solely on investigating the influence of the diffuser angle, excluding separators and end plates. CFD was employed to analyze the aerodynamic characteristics of a simplified sedan at various diffuser angles, including 0°, 3°, 6°, 9.8°, and 12°, with the original model having a 9.8° diffuser angle. The findings revealed that increasing the diffuser angle led to substantial changes in the underbody flow and wake, resulting in corresponding pressure changes. Consequently, the total aerodynamic drag coefficients of the car initially decreased and then increased, while the total aerodynamic lift coefficients decreased [9].

The working principle in this study is based on Bernoulli's Fluid Flow principle. Different velocities at various points around the wing cross-section cause a varying pressure distribution at every point around the body according to the Bernoulli equation. When the wing section is curved,

the area on the upper surface is increased and the speed of the air passing over the section increases by increasing this area. By increasing the air velocity, the pressure is further reduced according to the Bernoulli equation. Thus, the pressure difference between the lower surface and the upper surface increases, and consequently the lift force is increased [10]. In their research, Selvam et al. (2023) studied laminar flow on a vehicle model under static circumstances. Boundary conditions were specified based on the New Car Assessment Program (NCAP) guidelines to make the experiment as realistic as feasible. Multiple simulations were performed using ANSYS Fluent while adjusting the experimental parameters, including fluid velocity, the vehicle's yaw angle, and fluid pressure. A notable downforce of 33% was achieved, and successful results led to the creation of the aero map [11]. In two examples where their coefficients from the analysis were acquired, Ipilakyaa et al. (2018) studied drag and lift forces. Based on the findings, it was concluded that employing a rear spoiler with wings increased the downward force (negative lift), which in turn increased the car's drag. While the accompanying drag force results in greater fuel consumption, the additional downward force on the automobile will reflect in improved cornering abilities and high-speed stability. The advantages of employing the rear spoiler exceed those of not using it based on the amount of downward force created in comparison to drag force and provided that safety comes before moving faster [12].

Companies are making considerable investments in Formula 1 cars. Therefore, the most advanced technologies in the automotive industry around the world are used on these vehicles. Because the Research and Development (R&D) and investment costs are very high, the impact of the drag and downforce forces in races is of great importance. It is critical to choose the proper airfoil and place it at the proper angle in a way that will be most efficient in this sector, where even the spoiler can make a difference. The subject of this study is to examine the effect of the selection and positioning of the airfoil profile in the spoilers of today's Formula 1 vehicles at different speeds on the friction coefficient, downforce coefficient, and downforce with the Computational Fluid Dynamics (CFD) program. Therefore, the size of the Downforce that the selected two airfoils will create at different speeds and angles of attack depending on Drag coefficient (C_D) and Lift coefficient (C_L) values were also analyzed. In this study, unlike other literature studies, a different standard, BE153 coded profiles were used instead of National Aviation Advisory Committee (NACA). The reason for this is to be able to evaluate and comment on these profiles used in the F1 racing car industry. In addition, this study aims to observe the effect of downforce at different speeds by using different

profiles and angles of attack within the same evaluation. Thus, it has been observed that the profiles placed at what speed and at which angle are the most suitable options according to the need.

2. MATERIALS AND METHODS

The numerical study was carried out using the ANSYS Fluent commercial program. The three-dimensional profiles are built on the Solidworks program. Subsequently, in necessary cases, analyses were carried out by determining the boundary conditions. The results were also measured in Newton units along with the C_D and C_L coefficients. 12 different situations are based on two different airfoil profiles, two different angles of attack, and three different velocities. The parameters of all analyses performed are given in Table 1.

Table 1. Parameters of the analyses

Airfoil	Angle of Attack(°)	Velocity (m/s)
BE153-055	10	30
BE153-055	10	50
BE153-055	10	70
BE153-055	20	30
BE153-055	20	50
BE153-055	20	70
BE153-175	10	30
BE153-175	10	50
BE153-175	10	70
BE153-175	20	30
BE153-175	20	50
BE153-175	20	70

2.1. Creation of Geometry

The coordinates of the profiles to be used when creating geometry were taken and first drawn in two dimensions. Subsequently, profiles of 0.8 meters of spoiler width in an F1 car were changed to three dimensions. In the next step, the two spoilers created were placed so that the attack angle would be 10 and 20 degrees. A total of four solid models were created for the analyses. The views of solid models, BE153-175, with a 10° angle of attack are given in Figure 1 as an example.
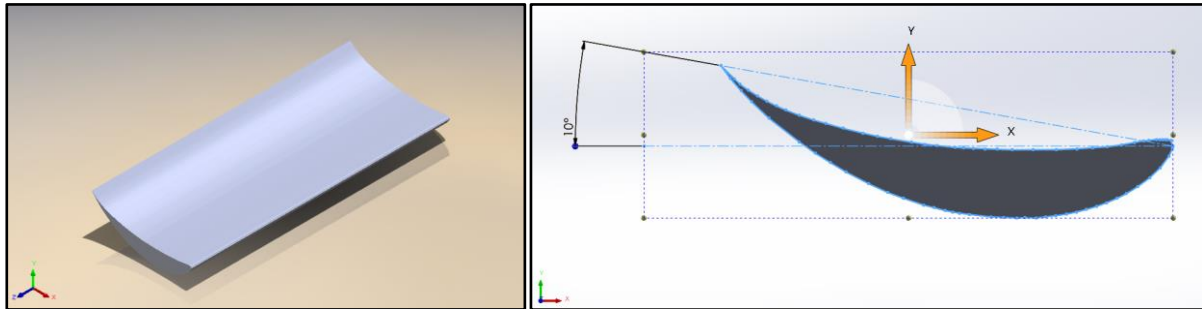
Figure 1. The views of solid models, BE153-175, 10° angle of attack

2.2. Meshing Process

The meshing process was applied to four three-dimensional geometries for the analyses. First, the default mesh was set. The default mesh had 2379 nodes and 10994 elements. The lowest element quality was around 9×10^{-4}. The element size was 0.234 m. Afterward, the values were increased by making improvements to the mesh. With the sizing command, the element sizes on the mesh were reduced to 0.03 m. Then capture curvature and capture proximity were added. The smoothing option in the quality option was selected as high. The default mesh was improved by adding automatic methods. In addition to these, the inflation method was used. The average skewness value is around 0.23. This value is within the acceptable limit for fluent analysis [13]. On the other hand, as a result of the improvements, it has 926755 nodes and 3286380 elements. The mesh images and mesh values of the BE173-175 airfoil used in the analysis are given in Figure 2. Also, views of the mesh structure created are given in Figure 3.

Figure 2. Mesh statics

Figure 3. The generated mesh structure

2.3. The Equations Used by CFD Program

To simulate the three-dimensional motion of a fluid particle, the Navier-Stokes equations are employed. These equations will be provided in the upcoming subsections.

2.3.1. Conservation of mass

The mass conservation for a particle having dimensions of dx, dy, and dz is expressed with Equation 1.

$$\frac{\partial \rho}{\partial t} + \frac{\partial (\rho u_i)}{\partial x_i} = 0 \tag{1}$$

2.3.2. Conservation of momentum

The law of conservation of momentum is essentially a manifestation of Newton's second law of motion. It asserts that the rate of change of momentum of a system over time is equal to the sum of external forces acting upon that system. This principle can be mathematically expressed using Equation 2.

$$\frac{D(u_i)}{Dt} = \frac{\partial u_i}{\partial t} + u_J \frac{\partial u_i}{\partial x_J} = -\frac{1}{\rho} \frac{\partial P}{\partial x_i} + v \frac{\partial^2 u_i}{\partial x_j^2} + F_i \tag{2}$$

The external flow field around a spoiler is modeled and simulated using the Reynolds Averaged Navier-Stokes (RANS) equations. RANS methods find extensive application in various industrial contexts. These equations, specifically for the x, y, and z axes, are provided in Equation 3.

x – component:

$$\rho \frac{D\bar{u}}{Dt} = \rho \left[\frac{\partial}{\partial x}(\bar{u}^2) + \frac{\partial}{\partial y}(\bar{u}\bar{v}) + \frac{\partial}{\partial z}(\bar{u}\bar{w}) \right.$$

$$= \rho g_x - \frac{\partial \bar{P}}{\partial x} + \frac{\partial}{\partial x}\left[\mu \frac{\partial \bar{u}}{\partial x} - \rho \overline{u'^2} \right] + \frac{\partial}{\partial y}\left[\mu \frac{\partial \bar{u}}{\partial y} - \rho \overline{u'v'} \right] + \frac{\partial}{\partial z}\left[\mu \frac{\partial \bar{u}}{\partial z} - \rho \overline{u'w'} \right]$$

y – component:

$$\rho \frac{D\bar{v}}{Dt} = \rho \left[\frac{\partial}{\partial x}(\bar{u}\bar{v}) + \frac{\partial}{\partial y}(\bar{v}^2) + \frac{\partial}{\partial z}(\bar{v}\bar{w}) \right.$$

$$= \rho g_y - \frac{\partial \bar{P}}{\partial y} + \frac{\partial}{\partial x}\left[\mu \frac{\partial \bar{v}}{\partial x} - \rho \overline{u'v'} \right] + \frac{\partial}{\partial y}\left[\mu \frac{\partial \bar{v}}{\partial y} - \rho \overline{v'^2} \right] + \frac{\partial}{\partial z}\left[\mu \frac{\partial \bar{v}}{\partial z} - \rho \overline{u'w'} \right] \tag{3}$$

z – component:

$$\rho \frac{D\bar{w}}{Dt} = \rho \left[\frac{\partial}{\partial x}(\bar{u}\bar{w}) + \frac{\partial}{\partial y}(\bar{v}\bar{w}) + \frac{\partial}{\partial z}(\bar{w}^2) \right.$$

$$= \rho g_z - \frac{\partial \bar{P}}{\partial z} + \frac{\partial}{\partial x}\left[\mu \frac{\partial w}{\partial x} - \rho \overline{u'w'} \right] + \frac{\partial}{\partial y}\left[\mu \frac{\partial \bar{w}}{\partial y} - \rho \overline{v'w'} \right] + \frac{\partial}{\partial z}\left[\mu \frac{\partial \bar{w}}{\partial z} - \rho \overline{w'^2} \right]$$

2.4. The Boundary Conditions

The regions used to define the boundary conditions are given in Figure 4. In Figure 4, the blue region represents the inlet, the red represents the outlet, and the yellow parts represent the walls. The green part is the spoiler wall.
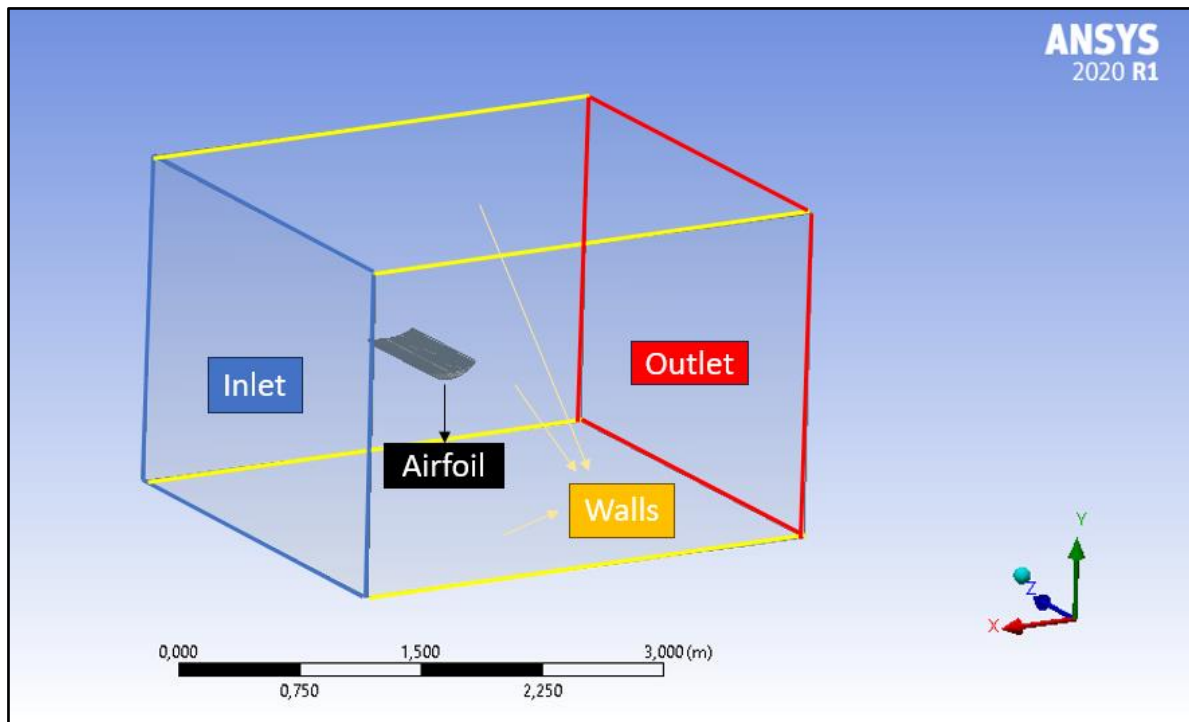
Figure 4. The regions used for setting up the boundary conditions for the CFD analyses

The assumptions made during the analysis are as follows:

1. It is assumed that the flow is incompressible, so the Pressure-Based simulation has been carried out.

2. Although the Navier-Stokes equations have been simplified, solving them analytically is still impossible, despite the procedure with conservation equations and averaging. Therefore, a turbulence model is required to solve the two equations accurately for the flow. In this study, the k - ω SST model is used in addition to the RANS equations. This model is best suited for aerospace applications where strong back pressure gradients and separation are observed. Although the standard k - ω model overestimates separation, the k - ω SST overcomes this problem. The use of the k - ω SST makes the model directly applicable from the boundary layer region to the viscous substrate. This formulation overcomes the overestimation of the model by switching to k - ε behavior in free flow [14].

3. The air is selected as fluid and its density is accepted as a value at a temperature of 15°C.

4. The speed is entered according to the parameters determined for the surface air input to be defined as inlet.

5. The pressure value in the area we selected for the outlet part is atmosphere so there is no effect of the pressure.

6. The speed on the airfoil surface is zero. No Slip Condition and the airfoil is stable.

7. The speed value at the zero point of the specified limit volume in contact with air is zero. No Slip Condition applies.

8. The value used to calculate the C_D value is entered in the field part of the reference values. This value is the cut area that the airfoil looks at from the front. The speed indicated is the speed of the inlet part of the air.

9. Hybrid initialization has been used as a result of the non-divergence when previously resolved by standard initialization. In the primary assignment method, hybrid is the creation of starting conditions using boundary conditions and potential flow. This way, without the flow being deformed, a certain way reduces the risk of diverging the analysis, as it is the solution obtained with the acceptance of follow-up ethics [15].

10. The number of iterations is entered as 300 to approximate the analysis and correctly obtain the desired values. But, it converged at nearly the 100th iteration.

2.5. C_D and C_L Equations

The assessment of the drag coefficient (C_D) and the aerodynamic testing of vehicles typically involves a comprehensive process, encompassing computer simulations, small-scale wind tunnel experiments utilizing model cars, and culminating in trials conducted within large-scale wind tunnels, employing full-scale prototypes that faithfully replicate the dimensions of the actual vehicles. The term "Drag Coefficient" can also be called the "Wind Resistance Coefficient," and it is commonly denoted by abbreviations such as C_w, C_D, and C_x. Its mathematical expression is defined by Eq. 4. where ρ represents air density, v represents the object's velocity relative to the surrounding air, and A represents the frontal projected area of the object. In Eq. 4. F_D corresponds to the drag force [4].

$$C_D = \frac{F_D}{\frac{1}{2} \times \rho \times v^2 \times A} \tag{4}$$

The lift coefficient (C_L), which is a dimensionless number used in fluid dynamics, connects the lift produced by a lifting body to the fluid density surrounding it, the fluid velocity, and a related reference region. The angle of the body to the flow determines C_L. The coefficient of section lift The term "C_L" describes the dynamic lift properties of a two-dimensional foil section, where the foil chord serves as the reference region. C_L is provided by Eq. 5. A is the frontal projected area of the airfoil, v is the object's speed in relation to the liquid, is the air density, and F_L is lift force.

$$C_L = \frac{F_L}{\frac{1}{2} \times \rho \times v^2 \times A}$$ (5)

3. RESULTS AND DISCUSSIONS

The results of the analysis were thoroughly examined in this section, with a special emphasis on the precise visual evaluation of pressure contours. The differences in C_D (drag coefficient), C_L (lift coefficient), and downforce coefficients across various situations were also examined using a comparative study. The main goal of these numerical approaches was to improve our understanding of the study findings within the constraints of the experimental settings. The visual evaluation of changes in pressure contours acts as a vital tool for acquiring a deeper understanding of the complexities of fluid flow behavior when digging into the study of the analysis findings. Additionally, evaluating the effectiveness of the designed or tested object requires a detailed understanding of how coefficients like C_D and C_L change in response to shifting situations. The quantification of downforce, conversely, plays a critical role in ascertaining the degree to which an aerodynamically controlled object experiences a downward force acting upon it in relation to the ground.

3.1. Mesh Independence

This research is entirely based on a numerical approach, meaning that experimental data has not been utilized. Instead, results have been obtained through computer-based simulations and calculations. Such an approach requires a specific step to verify the accuracy and reliability of the analyses. This verification step is referred to as the mesh independence test. Mesh independence tests involve running simulations with different resolutions of the computational mesh to determine how consistent the results are and how much they change as the resolution increases. In other words, using a finer mesh or higher resolution computational mesh can enhance the accuracy of the results but may also extend the computational time [16]. Therefore, it is emphasized that this study relies on numerical methods and mesh independence tests were conducted to ensure the reliability of the results. The results of C_D and C_L coefficients in different mesh structures are given in Table 2.

Table 2. C_D and C_L coefficients in different mesh structures

Element Number [x10^3]	Drag Coefficient(C_D)	Lift Coefficient (C_L)
4146	0,3371	1,8064
3286	0,3382	1,8106
2064	0,3355	1,7981
498	0,3281	1,8435

To verify mesh independence, analyses were conducted using four different mesh structures for BE153-175, angle of attack 10°. The aim was to ensure that C_D and C_L values converged as a result of these analyses. When examining the analyses with 3 million and 4 million elements, it was observed that the difference in C_D values was around 0.3%, while the difference in C_L values was approximately 0.2%. Consequently, a mesh structure with 3 million elements was chosen for the analyses. Therefore, opting for 3 million elements instead of 4 million elements is a more practical choice to save computational time and resources.

3.2. Pressure and Velocity Contours

When examining the pressure contours, the parts with high pressure are shown in red, representing high pressure. The parts with low pressure are shown in green colour which represents low pressure. This shows us that the downforce is formed successfully. At the same time, we can see the change of pressure differences according to the color change. The pressure and velocity contours for BE153-175, angle of attack 10° are given in Figure 5 and 6.
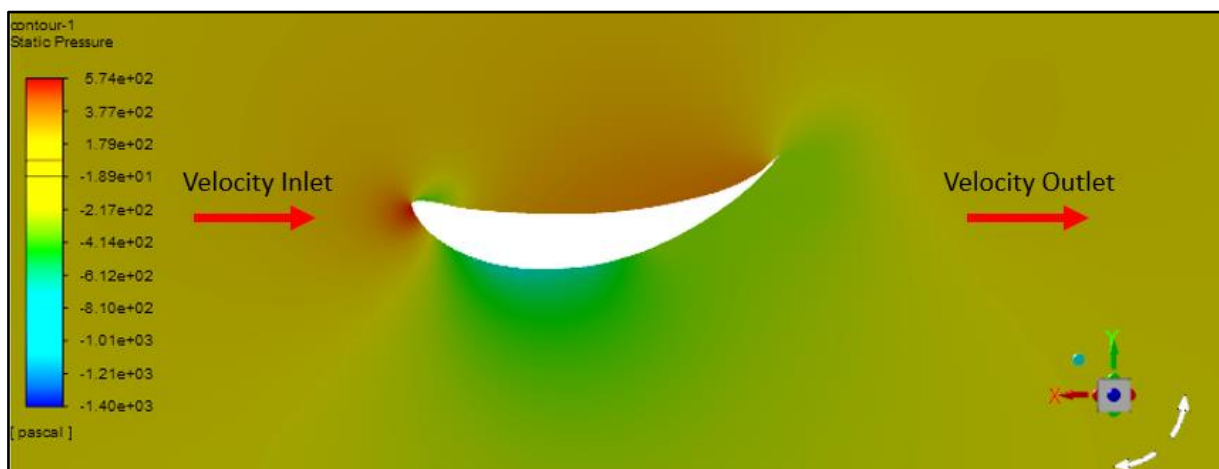
Figure 5. The pressure contour
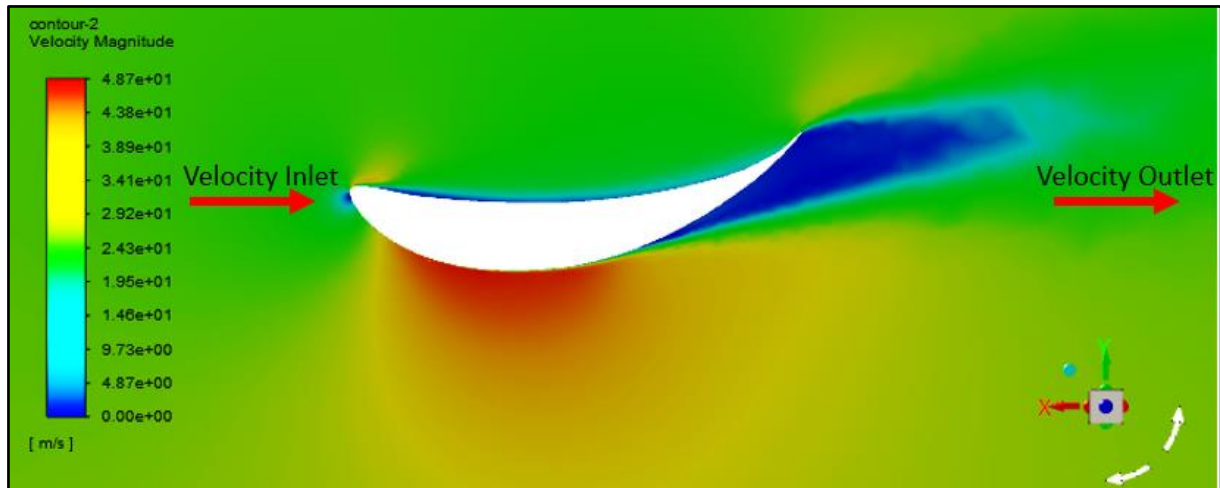
Figure 6. The velocity contour

3.3. Downforce Values

The effect of wing profiles and angle of attack on downforce is given in Figure 7. When the downforce value according to the speed changes, which is the first of the parameters, is examined, the downforce force for the BE055-10° profile was measured as 114.069 N at a speed of 30 m/s. When the speed increased to 50 m/s, 318.54 N and 626.104 N downforce force was obtained at 70 m/s. When the angle of attack, another parameter, is examined, the BE153-175 profile was analyzed at a speed of 30 m/s with an angle of attack of 10°, and the downforce value was determined as 183.392 N. When we analyzed the same profile structure at the same speed but at 20° angle of attack, it was observed that it produced a downforce of 248,871 N. Finally, when analyzed at 20° angle of attack, 70 m/s speed but different profiles, the BE153-055 profile produced a downforce of 981,827 N. At the same angle of attack and speed, the BE153-175 profile produced a downforce of 1377.112 N. As seen in Table 3 and Figure 7, the downforce force is directly proportional to the camber line of the wing profile, the angle of attack, and the vehicle's speed.
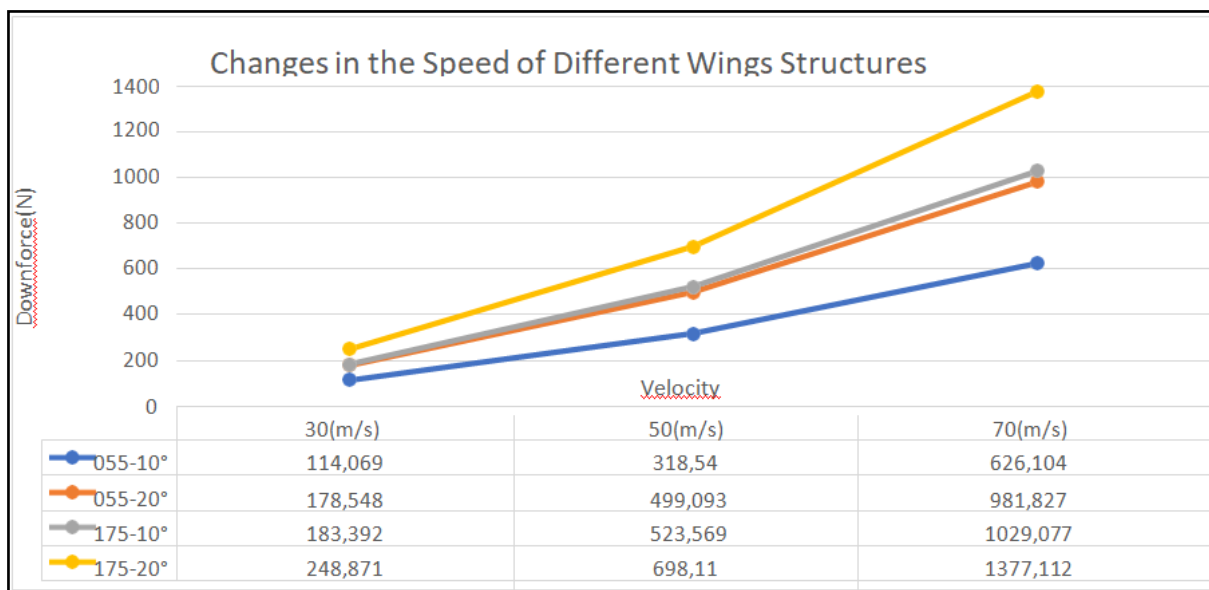
Figure 7. The changes in the speed of different wing structures

3.4. C_D, C_L, and C_D/C_L Values

The C_D, C_L, and C_D/C_L values calculated after analysis in Table 3 are listed for different airfoil types and attack angles. As seen in Table 3, the C_D coefficient increased in direct proportion to the camber line and angle of attack. While the C_D coefficient of the BE153-055 airfoil with 10° angle of attack was 0.1301, the C_D coefficient of the BE153-175 airfoil with 10° angle of attack increased to 0.3382. At the same time, the C_L coefficient also increased in direct proportion to the camber line and angle of attack. Regarding the angle of attack, while the C_L coefficient of the BE153-055 airfoil with 10 degrees angle of attack was 1.1186, the C_L coefficient of the BE153-175 airfoil with 10° angle of attack increased to 1.8106. In terms of angle of attack, while the C_L coefficient of the BE153-055 airfoil with 10° angle of attack was 1.1186, the C_L coefficient of the BE153-055 airfoil with 20° angle of attack increased to 1.7495. However, when the C_D/C_L values were examined, it was observed that the C_D coefficient increased more than the C_L coefficient. When we increase the angle of attack of the BE153-055 airfoil by 10°, the increase in the C_D coefficient is 138% while the increase in the C_L coefficient is 56.4%. In other words, when more downforce is desired to be provided, the increase in drag force will be greater than the downforce.

Table 3. The C_D, C_L and C_D / C_L values

Airfoil	Angel of Attack(°)	C_D	C_L	C_D/C_L
BE153-055	10	0,1301	1,1186	0,116306
BE153-055	20	0,3101	1,7495	0,177251
BE153-175	10	0,3382	1,8106	0,186789
BE153-175	20	0,5931	2,4471	0,242369

The results of the analysis showed that the airfoil produced downforce. The analysis shows that the values of C_D and C_L are equal when analyzed at different speeds using the same airfoil and attack angle. If we compare the airfoil cells, the higher the cells appear to be, the greater our C_L value also appears. As a result, the downforce has also increased. In addition to this, the value of the C_D has also increased. If we continue the comparison with the placement of the same airfoil at different attack angles, the higher the angle of attack, the higher the C_D and C_L values. Thus, it has been observed that this parameter is also associated with the field variable. Using the same airfoil and attack angle but at different speeds, it was observed that the speed did not affect the C_D and C_L values but also increased the downforce parabolically. If we examine the value of C_D/C_L, although we get more downforce force along with the increase in convulsion, C_D increased more than the proportional increase. As a result, even if we obtain more downforce force on a quantity basis, this value has decreased proportionally. When the change of the C_D/C_L value by the attack angle was examined, it was found that the size of the downforce force increased but that the proportional value of C_D increased more than the value of C_L.

4. CONCLUSION

When the C_D and C_L results are examined according to the analysis of the profiles in four structures, the profile with the lowest C_D coefficient is BE153-055 and the attack angle is 10 degrees. At the same time, the rate of C_L is at the lowest level. Therefore, the lowest downforce force is also taken in this case. The profile with the highest C_D coefficient is BE153-175 and the attack angle is 20 degrees, while the maximum C_D is still in this case.

When C_D/C_L values are examined, the most suitable wing profile is BE153-055 and the attack angle will be 10 degrees. But the maximum downforce that can be obtained in this case is 248,871

N at a speed of 70 m/s. So if more downforce force is needed, other wing profiles or attack angles should be selected.

On the other hand, the downforce values were analyzed in twelve different cases, and the results varied from 114,069 N to 1377,112 N depending on speed. As is understood here, choices in different structures and different angles of attack can be selected depending on the need and the downforce force desired to be obtained can be met depending upon these choices.

ACKNOWLEDGMENT

DECLARATION OF ETHICAL STANDARDS
The authors of the paper submitted declare that nothing which is necessary for achieving the paper requires ethical committee and/or legal-special permissions.

CONTRIBUTION OF THE AUTHORS
Muhammed Ali Oztemel: Construction of the model, consideration, and interpretation of the results, manuscript preparation, check of the paper template, and proofreading**.**

Fatih Aktas: Construction of the model, consideration and interpretation of the results, manuscript preparation, check of the paper template, and proofreading.

Nuri Yucel: Consideration and re-interpretation of the results, check of the paper template, and proofreading.

CONFLICT OF INTEREST
There is no conflict of interest in this study.

REFERENCES
[1] Vishwakarma YK, Saxena MR, Nagrajan PK. Aerodynamic improvement of car body. International Journal of Engineering Research & Technology 2014; 3(6): 1761-1763.

[2] Parab A, Sakarwala A, Paste B, Patil V, Mangrulkar A. Aerodynamic analysis of a car model using fluent Ansys 14.5. International Journal on Recent Technologies in Mechanical and Electrical Engineering 2014; 1(4): 07-13.

[3] National Transportation Safety Board. 2012. Crash During Experimental Test Flight, Gulfstream Aerospace Corporation GVI (G650), N652GD, Roswell, New Mexico, April 2, 2011. Aircraft Accident Report NTSB/AAR-12/02. Washington, DC.

[4] Bayındırlı C, Çelik M, Demiralp M. The investigation of flow characteristic around a bus model by CFD method and improvement of drag force by passive flow control method. Journal of Polytechnic 2018; 21(4): 785-795.

[5] Kazi A, Acharya P, Patil A, Noraje A. Effect of spoiler design on hatchback car. International Journal of Modern Trends in Engineering and Research 2016; 3(9): 192-200.

[6] Gorgulu YF, Ozgur MA, Kose R. CFD analysis of a NACA 0009 aerofoil at a low reynolds number. Journal of Polytechnic 2021; 24(3): 1237-1242.

[7] Guerrero A, Castilla R, Eid G. A numerical aerodynamic analysis on the effect of rear underbody diffusers on road cars. Applied Science 2022; 12.

[8] Widodo WA, Karohmah MN. CFD based investigations into optimization of diffuser angle on rear bus body. Applied Mechanics and Materials 2016; 836: 127-131.

[9] Hu X, Zhang R, Ye J, Yan X, Zhao Z. Influence of different diffuser angle on sedan's aerodynamic characteristics. Physics Procedia 2011; 22: 239–245.

[10] Erişen A, Bakirci M. Modifications of NACA 0012, NACA 4412 airfoils and analysis them by CFD. Journal of Engineering and Technological Sciences 2014; 50–82.

[11] Selvam MAJ, Kumar MR, Padmanabhan S, Subramanyam K, Reddy MN. Analyzing the downforce generated by rear spoiler of hatchback vehicle and creating an aeromapp using CFD analysis. Materials Today: Proceedings 2023; 92(1): 48-55.

[12] Ipilakyaa TD, Tuleun LT, Kekung MO. Computational fluid dynamics modelling of an aerodynamics rear spoiler on cars. Nigerian Journal of Technology 2018; 37(4): 975-980.

[13] Hammargren K. Aerodynamics modeling of sounding rockets. Ms. Thesis, Lulea University of Technology, 2018.

[14] Aytaç Z, Aktaş F. Utilization of CFD for the aerodynamic analysis of a subsonic rocket. Journal of Polytechnic 2020; 23(3): 879-887.

[15] ANSYS - Fluent User's Guide v17.1, 2017.

[16] Almohammadi KM, Ingham DB, Ma L, Pourkashan M. Computational fluid dynamics (CFD) mesh independency techniques for a straight blade vertical axis wind turbine. Energy 2013; 58.